Fish Gill Inspired Crossflow for Efficient and Continuous Collection of Spilled Oil

Journal:	*ACS Nano*
Manuscript ID	nn-2016-07918v.R1
Manuscript Type:	Article
Date Submitted by the Author:	08-Jan-2017

Complete List of Authors:	Dou, Yuhai; Institute for Superconducting and Electronic Materials, Australian Institute for Innovative Materials, University of Wollongong Tian, Dongliang; Beihang University, Sun, Ziqi; Queensland University of Technology, School of Chemistry, Physics and Mechanical Engineering Liu, Qiannan; Institute for Superconducting and Electronic Materials, Zhang, Na; Beihang University Kim, Jung Ho; University of Wollongong, Institute for Superconducting and Electronic Materials Jiang, Lei; The Chinese Academy of Sciences, Institute of Chemistry Dou, Shi Xue; University of Wollongong, ISEM

Fish Gill Inspired Crossflow for Efficient and Continuous Collection of Spilled Oil

Yuhai Dou,[†] Dongliang Tian,[‡] Ziqi Sun,*[†,§] Qiannan Liu,[†] Na Zhang,[‡] Jung Ho Kim,[†] Lei Jiang,[‡,⊥] and Shi Xue Dou[†]*

[†]Institute for Superconducting and Electronic Materials, Australian Institute for Innovative Materials, University of Wollongong, Wollongong, New South Wales 2500, Australia

[‡]Key Laboratory of Bio-Inspired Smart Interfacial Science and Technology of the Ministry of Education, School of Chemistry and Environment, Beihang University, Beijing 100191, P. R. China

[§]School of Chemistry, Physics and Mechanical Engineering, Queensland University of Technology, Brisbane, Queensland 4001, Australia

[⊥]Technical Institute of Physics and Chemistry, Chinese Academy of Sciences, Beijing 100191, P. R. China

ABSTRACT: Developing an effective system to clean up large-scale oil spills is of great significance due to their contribution to severe environmental pollution and destruction. Superwetting membranes have been widely studied for oil/water separation. The separation, however, adopts a gravity-driven approach that is inefficient and discontinuous due to quick fouling of the membrane by oil. Herein, inspired by the crossflow filtration behavior in fish gills,

we propose a novel crossflow approach via a hydrophilic, tilted gradient membrane for spilled oil collection. In crossflow collection, as the oil/water flows parallel to the hydrophilic membrane surface, water is gradually filtered through the pores, while oil is repelled, transported, and finally collected for storage. Owing to the selective gating behavior of the water-sealed gradient membrane, the large pores at the bottom with high water flux favor fast water filtration, while the small pores at the top with strong oil-repellency allow easy oil transportation. In addition, the gradient membrane exhibits excellent anti-fouling properties due to the protection of the water layer. Therefore, this bioinspired crossflow approach enables highly efficient and continuous spilled oil collection, which is very promising for the cleanup of large-scale oil spills.

KEYWORDS: fish gill, gradient, superhydrophilic, crossflow, oil spill

Oil spill events, such as the recent spill in Galveston Bay and the Deepwater Horizon oil spill in the Gulf of Mexico, result in severe damage to the environment and threats to human well-being.[1-4] Conventional clean-up technologies, *e.g.* skimmers,[5] sorbents,[6] controlled burning,[7] chemical dispersion,[8] and bioremediation,[9] suffer from either low efficiency or secondary pollution.[10,11] In view of this, great efforts have been devoted to developing superwetting materials by manipulating their microstructures[12-15] and surface chemistry,[16-19] which usually possess contrasting wettability towards water and oil, and therefore enable selective oil adsorption[20-23] or oil/water filtration.[24-30] Among them, superhydrophilic and underwater superoleophobic membranes have been widely developed for water-removal type separation by applying a perpendicular gravity-driven approach.[31-37] This perpendicular approach, however, suffers from the intrinsic limitation that the membrane pores are easily clogged by oil, leading to rapid decline of water flux and discontinuity of separation, which is inefficient for cleaning up

large-scale oil spills. Therefore, some more affordable and feasible innovations are still urgently demanded.

Nature offers us an alternative and distinctive idea, with the separation taking place in a parallel, not perpendicular way. One typical example is the crossflow filtration in suspension-feeding fishes, where the gradient gill structure can effectively collect tiny food particles from parallel flow of the suspension fluid by quickly eliminating water through the spaces.[38-41] This crossflow configuration also exists in human organs, such as the removal of airborne viruses and bacteria by the nasal membranes,[42] and the filtration of excess organic molecules from the blood by the kidneys.[43] Inspired by these natural processes, growing attention has been devoted to the development of micro/nano sciences and technologies for efficient separation through the crossflow approach.[44,45] Yobas's group designed four types of silicon-based microfilters, including weir, pillar, crossflow, and membrane, for isolation of white blood cells from red ones.[46] The result showed that the crossflow microfilter outperformed the others and exhibited the highest blood passing capacity, white-blood-cells trapping efficiency, and red-blood-cells passing efficiency. Ismail's group prepared a nanocomposite membrane with holloysite nanotube clay nano-filter embedded into the polyvinylidene fluoride polymer matrix and studied its antibacterial properties in a crossflow ultrafiltration system.[47] This nanocomposite membrane could effectively remove two types of bacteria from contaminated water with high permeation flux and excellent anti-fouling properties, thus exhibiting a great potential for antibacterial applications. Considering these progresses made in micro/nano sciences, the realization of oil/water separation in a crossflow approach should be a promising strategy for cleaning up oil spills. Herein, we successfully introduce this crossflow configuration to the collection of spilled oil by using a hydrophilic and tilted gradient membrane. In crossflow collection, oil/water flows

parallel to the membrane surface, during which water is quickly filtered through the large-pore region, while oil is strongly repelled and effectively collected in the small-pore region. The collection efficiency and continuity of this crossflow approach are determined by a water layer that seals the membrane pores, which not only presents different gating behaviors towards water and oil, but also endows the membrane with excellent anti-fouling properties. Via a laboratory-scale device, we have verified that this crossflow approach enables highly efficient and continuous spilled oil collection, showing its great potential in cleaning up large-scale oil spills.

RESULTS AND DISCCUSION

In nature, the ever-present adaptive structures endow biological species with amazing functions to survive in harsh environments. For some fish species, the unique suspension-feeding behavior is accomplished by their filter-like gradient gill structure that is formed by the lateral gill arches, longitudinal gill rakers and central spaces (Figure 1a).[38] This special gill structure has been assumed to function as a dead-end filter, sieving suspended particles from perpendicular flow of the suspension fluid. However, it is easily clogged by food particles through the dead-end approach, leading to rapid decline of filtration efficiency (Figure S1a). To prevent that from happening, the gill structure actually functions via a remarkably alternative mechanism, namely crossflow filtration, which allows the suspension fluid to flow parallel, rather than perpendicularly, to the gill surface (Figure 1b). In crossflow filtration, nearly all food particles travel towards the oesophagus without touching the gill surface, effectively avoiding the clogging of the filter and achieving high-efficient filtration (Figure S1b).[41]

Inspired by the crossflow filtration behavior in fish gill, we propose a novel strategy for oil spill cleanups—crossflow spilled oil collection. This strategy is accomplished by a gradient

membrane that mimics the gill structure of suspension-feeding fishes. It consists of five meshes arranged in descending order of pore size from the bottom to the top (150, 120, 90, 60 and 30 μm, as shown in Figure 1c,d and Table S1). In order to improve the hydrophilic property of the membrane, ultrathin Co_3O_4 nanosheets were uniformly coated on its surface via a facile hydrothermal method (Figures 1e and S2).[48] As can be seen, these ultrathin nanosheets intertwine with each other and form numerous enclosed cells. Figure 1f schematically depicts the fish gill inspired crossflow spilled oil collection. In this crossflow concept, the gradient membrane is installed on a power-driven system (*e.g.* a ship) with large pores at the bottom and small pores at the top. When the ship moves at an appropriate speed, both water and oil are driven onto the membrane and flow in a parallel direction along the membrane surface, during which water gradually passes through the pores, while oil travels with the crossflow and is finally collected for storage. The key to this crossflow design lies in a water layer that covers the gradient membrane surface. The water-sealed membrane presents highly selective gating behavior that allows the quick permeation of water at the large pore region but blocks the permeation of oil at the small pore region. Moreover, the sealing water layer minimizes the direct contact between the membrane surface and the oil fluid, endowing the membrane with excellent anti-fouling properties. As a result, this bioinspired crossflow approach enables highly efficient and continuous spilled oil collection.

Because the extreme state of the water-sealed membrane (the case of a wetted membrane with water just filling in the pores) is the weakest point in terms of repelling the oil and preventing its permeation, we first carried out some basic theoretical researches on its formation and oil-repellency. The formation was evaluated by studying the spreading behavior of a water droplet (1 μL, dyed with Rhodamine B) on the five component parts of the gradient membrane.

Due to the superhydrophilicity of the Co_3O_4-coated wires (Figure S3) and the hydrophobicity of the pores, a capillary driving force and a pinning force are applied on the droplet and control its spreading. As a result, three distinct states are yielded with decreasing pore size: no spreading, partial spreading and full spreading (Figure 2a,b). To better understand the spreading behavior in a more realistic system, we simplify the complex braided structure to two perfectly parallel wires (Figure 2c), such that the equilibrium conditions for different states can be approximately given according to the minimization of surface energy (see Figure S4 for the derivation):[49]

$$(R_1/r)^2[\pi/2 - \theta_1 - \alpha_1 + \sin(\theta_1 + \alpha_1)\cos(\theta_1 + \alpha_1)] + 2(R_1/r)[\sin\alpha_1\cos(\theta_1 + \alpha_1) - \alpha_1\cos\theta_1] + \sin\alpha_1\cos\alpha_1 - \alpha_1 = 0 \quad (1)$$

where R_1 is the curvature of the water surface, r is the radius of the wire, θ_1 is the water contact angle on the wire surface, and α_1 is the angle between the line connecting the wire centers and the radius to the air-water-solid boundary. In Equation (1), R_1/r can be replaced by:

$$R_1/r = (1 + d/2r - \cos\alpha_1)/\cos(\theta_1 + \alpha_1), (d, \text{pore size}) \quad (2)$$

Therefore, a relationship is established among $d/2r$, θ_1 and α_1. Since $\theta_1 = 0°$ (Figure S3), we obtain that: when $d/2r > \sqrt{2}$ (150, 120 and 90 μm membranes, Table S1), $\alpha_1 = \pi$ and the spreading does not happen; when $0.57 < d/2r < \sqrt{2}$ (60 μm membrane), $\pi/2 < \alpha_1 < \pi$ and partial spreading occurs; when $d/2r < 0.57$ (30 μm membrane), $\alpha_1 < \pi/2$ and full spreading takes place.[49,50] These analyses are consistent with our experimental results, indicating the easier formation of the sealing water layer on small-pore membranes.

The oil-repellent property of the water-sealed membrane was then evaluated by studying the spreading behavior of an oil droplet (anti-wear hydraulic fluid, 5 μL) on membranes with different pore sizes. As shown in Figure 2d, the spreading area decreases with decreasing pore size, which is mainly attributed to the strong pinning effect of the water-wetted wires in the

lateral direction and the enhanced oil-repellency of the water layer in the vertical direction. The lateral pinning effect is detailedly interpreted in Figure S5. Here, we mainly focus on the oil-repellency of the water layer, and the mechanism is schematically shown in Figure 2e, where the repellent force (P) can be evaluated according to the Laplace law:[51]

$$P = \Delta P = 2\gamma_{L_1L_2}/R_2 = 4\gamma_{L_1L_2}\sin(\theta_2 - \pi/2 - \alpha_2)/D \quad (3)$$

where ΔP is the oil pressure, $\gamma_{L_1L_2}$ is the surface tension of the oil-water interface, R_2 is the curvature of the meniscus, θ_2 is the advancing contact angle of oil on the wire surface, α_2 is the angle between the line connecting the wire centers and the radius to the oil-water-solid boundary, and D is the distance between the two oil-water-solid boundaries. From simple geometry, it follows:

$$D = 2r(1 - \cos\alpha_2) + d \quad (4)$$

Therefore, a decrease in d leads to an increase in P, indicating that stronger oil-repellency can be achieved by the sealing water layer on small-pore membranes.

Based on the aforementioned theoretical analyses on the formation and oil-repellency of the water-sealed membrane, the wetting and permeating behaviors of water and oil on the membranes were investigated. As shown in Figure 3a, a water droplet can easily penetrate through the pores and wet both sides of the membrane due to the superhydrophilicity of the wires. This wetting behavior is more apparent for large-pore membranes because of their high porosity. The water contact angle decreases with decreasing pore size (Figure 3b), confirming the easier formation of the sealing water layer on small-pore membranes. In comparison, an oil droplet cannot penetrate easily through the pores once they are sealed with water (Figure 3c).[52] The oil contact angle increases with decreasing pore size (Figure 3d), signifying the enhanced oil-repellency of the water-sealed membrane. The contrasting wetting behavior between water and

oil suggests that the sealing water layer acts as a selective gating liquid with respect to the permeability of the membrane, which allows the permeation of water (Figure 3e) but prevents the permeation of oil (Figure 3f). The selectivity of the water-sealed membrane is greatly influenced by its pore size. By decreasing the pore size from 150 to 30 μm, the water flux declines gradually from 265 to 50 L m^{-2} s^{-1}, while the oil breakthrough pressure (*e.g.* diesel) rises dramatically from 0.71 to 3.90 kPa.

Owing to the opposite permeating behavior between water and oil, the crossflow design enables selective collection of oil by eliminating water through the pores. In crossflow collection, the sealing water layer evolves from overlying on the surface to being trapped in the pores (Figure 4a). The overlying layer covers most of the membrane and creates a smooth water surface. Therefore, oil is isolated from the membrane and floats freely on it (Figure 4b).[53,54] In contrast, the pore water layer exists only in the top part and causes a rough water/solid surface. As a result, oil comes into contact with the membrane and slides with difficulty over it.[55] We evaluated the oil-floating stage by measuring the height that a water current (0.5 cm in thickness) could climb on the tilted membranes. As can be seen in Figure 4c and d, the climbing height of the water current increases with decreasing pore size due to the decline in water flux. In addition, the increase of the current speed and the membrane tilt also lead to the increase of the climbing height. The oil-sliding stage was then characterized by depositing an oil droplet (20 μL) on the tilted and water-sealed membranes (Figure 4e). As expected, oil slides much more easily on small-pore membranes due to their stronger oil-repellency. These studies emphasize the importance of the sealing water layer in facilitating the oil transportation and collection during the crossflow process. They also suggest that in practical applications the oil storage container should be adjusted to an appropriate height according to the changes in pore size, ship speed and

membrane tilt, so as to maximize the floating stage while minimizing the sliding stage, as long as water does not flow into the container (Figure 1f).

From the above characterizations of oil/water wettability, permeability and mobility, we can conclude that the water-sealed gradient membrane plays a continuously adaptive role in crossflow spilled oil collection. In the beginning, with a great deal of water flowing onto the membrane, the large pores at the bottom with high water flux enable fast water filtration. In the end, as water is filtered out and oil comes into contact with the membrane, the small pores at the top are conducive to the formation of the sealing water layer, which not only prevent oil penetration, but also facilitate oil transportation. It is also worth noting that the ultrathin Co_3O_4 nanosheets coated on the wire surface also contribute to the oil collection (Figure S6 and Table S2). Unlike previously reported open structures,[30-32,35] these nanosheets intertwine with each other, forming numerous enclosed cells (Figure 1e). These cells firmly lock water inside and generate a robust repelling layer. In this way, oil is easily transported and collected (Figure S7).

Based on the proposed crossflow collection of spilled oil, a laboratory-scale demonstration device that consists of an inclined gradient membrane and an oil container was designed as a proof of concept (Figure 5a). An apparatus was also fabricated with water and crude oil filling in a rectangular sink to simulate an environmental oil spill (Figure S8). For the demonstration, the device was installed on the apparatus and controlled to move along the crude oil/water interface (Figure 5b). As expected, the oil/water flows parallel to the membrane surface with water gradually permeating through the pores, while the crude oil is transported with the crossflow and finally collected in the container.

Due to the limited dimensions of the apparatus on the laboratory scale, the performance of the device could not be exactly determined in one go. Therefore, we controlled the device to

continually and repeatedly collect the spilled oil (Methods and Table S3), and statistically evaluated its collection efficiency (Q) according to the following equation:

$$Q = V/(W*t) \quad (5)$$

where V is the collected oil volume, W is the membrane width, and t is the cumulative collection time. As shown in Figure 5c, the initial collection efficiency for the crude oil reaches 52.2 L m^{-1} min^{-1} at a device speed of 0.4 m s^{-1}. Other types of oil, such as diesel, corn oil and anti-wear hydraulic fluid, could also be collected with initial efficiencies above 50 L m^{-1} min^{-1}, suggesting the universality and practicality of this crossflow approach in cleaning up various oil spills. More remarkably, the collection efficiencies for these oils suffer from only a tiny decline of 1.3−2.9% after a cumulative collection time of 100 min (continual collection for more than 2000 times), significantly outperforming the gravity-driven approach (which losses its selectivity within 50 times, Figure S9). We also demonstrated that the gradient membrane (average pore size, 90 μm) exhibits much higher collection efficiencies compared with a single-pore-size membrane (90 μm) at different device speeds (Figure 5d). The outstanding performance of high efficiency and high continuity is mainly attributable to the water-sealed gradient membrane. On the one hand, the large pores at the bottom with high water flux favor fast water filtration, while the small pores at the top with strong oil-repellency allow easy oil transportation. On the other hand, the sealing water layer minimizes the direct contact between the membrane and the oil fluid, which endows the membrane with excellent anti-fouling properties. At last, to simulate the real environmental conditions, we studied the effect of surface waves on crossflow spilled oil collection. As shown in Figure S10, the collection efficiency declines much more quickly with increasing wave height, indicating the adverse effect of surface waves. Therefore, some measures should be taken in

practical applications to remove the water waves before collection or minimize its adverse effect by increasing the climbing height of oil/water mixture.

CONCLUSIONS

Our bioinspired crossflow concept, in which oil/water is driven to flow parallel to a gradient membrane surface, provides a novel approach for highly efficient and continuous spilled oil collection. This crossflow design also exhibits other advantages compared with the previously reported gravity-driven approach. First, the collection process is finished in one step, while a pre-separation lifting process is needed for the gravity-driven approach. Second, the collection rate depends on the speed of the ship, which can reach a very high level, whereas the separation rate for the gravity-driven approach is limited by the low water permeation speed due to gravity. Thirdly, the pore-size gradient, the ship's speed, and the membrane length and tilt can be adjusted properly in order to withstand harsh surface conditions, *e.g.* water waves. Therefore, this approach is very promising for cleaning up large-scale oil spills. Such a bioinspired crossflow concept by utilizing the different wetting and permeating behaviors of different phases could also be extended to other areas that need efficient separations, such as water purification using graded layers of sand to sequentially remove contaminants from large particulates to small suspended microorganisms, air purification via a membrane filter with gradient pore distribution for the efficient removal of $PM_{2.5}$, and blood dialysis with a gradient semipermeable membrane for progressive elimination of waste water and undesired solutes.

METHODS

Materails. 316L stainless steel meshes were used as the substrates for the coating membranes. Chemicals, including polyethylene-oxide–polypropylene-oxide–polyethylene oxide (PEO_{20}-PPO_{70}-PEO_{20}, Pluronic P123, M_w = 5,800), ethylene glycol (EG, 99.8%), cobalt(II) acetate tetrahydrate ($CoAc_2 \cdot 4H_2O$, 98%), and hexamethylenetetramine (HMTA, 99.0%) were purchased from Sigma-Aldrich. Deionized water (15 MΩ·cm resistivity), ethanol (Chem-Supply Pty. Ltd., absolute), and acetone (Chem-Supply Pty. Ltd., 99.5%) were used for reaction and cleaning. Crude oil (medium, ONTA, Inc, Ontario, Canada), toluene (Sigma-Aldrich, 99.8%), diesel (Diesel Center Australia Pty. Ltd.), corn oil, and anti-wear hydraulic fluid (HM46) were used as test liquids. Transparent plastics (PMMA), a guide rail (V-Slot), a timing belt (GT2 profile), and a stepper motor (Nema 17) were purchased to fabricate the apparatus for the demonstration of crossflow spilled oil collection.

Membrane Preparation. Ultrathin Co_3O_4 nanosheets were coated on the membrane via a facile hydrothermal method. 0.2 g Pluronic P123 was first dissolved in 3.0 g ethanol. Then 1.0 g H_2O and 12 mL EG were added to form a homogeneous solution. Next, 0.13 g $CoAc_2 \cdot 4H_2O$ and 0.07 g HMTA were added under vigorous stirring for 30 min. After that, the solution was transferred into a 45 mL autoclave with the stainless steel meshes put in the bottom. The hydrothermal reaction was carried out at 170 °C for 15 h. Finally, the coated membranes were taken out and calcinated at 400 °C for 3 min. Other nanostructured coatings were also prepared by varying the amount of H_2O addition (0, 0.5, 2.0 and 4.0 g) in the reaction solutions. The gradient membrane consists of five single-pore-size membranes (Table S1). They were tailored with the same length and their edges were clamped between two plates following a descending sequence in pore size. The total length of the gradient membrane is varied according to different test parameters.

Characterization. The morphology of the membranes and the coated nanostructures was observed with a scanning electron microscope (SEM, JSM-7500FA, JEOL, Tokyo, Japan). The phase was evaluated using a powder X-ray diffractometer (XRD, MMA, GBC Scientific Equipment LLC, Hampshire, IL, USA) with Cu K_α radiation. Water spreading was observed via a video microscope (M-8LCD, Shanghai, China). Water and oil contact angles were measured on an OCA20 machine (Dataphysics, Germany) under ambient conditions.

Spreading test. Water spreading test was performed by depositing a 1 μL water droplet (dyed with Rhodamine B) on the horizontally-placed membrane. For oil spreading test, the membrane was pre-wetted with water, a 5 μL anti-wear hydraulic fluid droplet was then deposited on its surface and allowed to spread. To avoid evaporation of the water layer and make sure its surface was still flat, the oil droplet was deposited within 10 s after wetting the membrane.

Permeability test. Water permeability test was carried out using a home-made apparatus under a constant water pressure of 0.15 kPa. The water flux (F) was calculated from $F = V/St$ (where V is the permeation volume, S is the exposed surface area of the membrane, and t is the permeation time). Oil permeability test was carried out using the same apparatus, with the constraint that the membrane was pre-wetted with water and used within 10 s. The oil breakthrough pressure (P) was calculated according to the equation: $P = \rho g h_{max}$ (where ρ is the density of oil, g is the acceleration due to gravity, and h_{max} is the maximum height of oil the membrane can support).

Mobility test. For the water climbing test, a water current with a thickness of 0.5 cm was generated and made to flow onto the tilted membrane. The climbing height was measured by varying the speed of the water current and the inclination angle of the membrane. Since oil sliding takes place on a rough surface with water trapped in the pores, we first wetted the membrane, and then left it for 10 min to evaporate some water and generate the pore water layer.

The water-sealed membrane was tilted at 30°, and a 20 μL droplet of anti-wear hydraulic fluid was deposited on its surface and allowed to slide. The average sliding speed was calculated after sliding for 20 s.

Demonstration of crossflow spilled oil collection. A laboratory-scale demonstration device was designed with a gradient membrane installed in the front with large pores at the bottom and small pores at the top (membrane tilt, 30°). The membrane is rectangular in shape with a fixed width and a variable length. A demonstration apparatus (dimensions, 1000 × 100 × 100 mm) was fabricated to provide the device with a good operating environment (Figure S7). To simulate an environmental oil spill, water and corn oil were poured into the apparatus, generating an oil layer 3 mm in thickness. For demonstration, the membrane was pre-wetted with water, which serves as a barrier layer for initial oil collection. The height (H) of the container above the oil/water interface was a little larger than the measured climbing height of the water current, so that water would not flow into the container. Here we set $H = 1.1h$ (Table S3). To evaluate the collection efficiency and stability, the speed of the device was set at 0.4 m s^{-1}. The volume of the collected oil was measured at every cycle, and then it was poured back to maintain the total oil content in the sink. The oil collection efficiency (Q) was calculated following the equation: $Q = V/(W*t)$, where V is the collected oil volume, t is the cumulative collection time, and W is the membrane width. For the stability test, the collection efficiency was obtained with a t-value of 10 min. The comparison between the gradient membrane (average pore size, 90 μm) and the single-pore-size membrane (90 μm) was carried out at different device speeds (0.3, 0.4, 0.5 and 0.6 m s^{-1}) with a t-value of 0.5 min. To simulate the real environmental conditions, artificial surface waves with different wave heights (1, 2 and 4 mm) were produced by air-blowing. All the data above were averaged from five measurements.

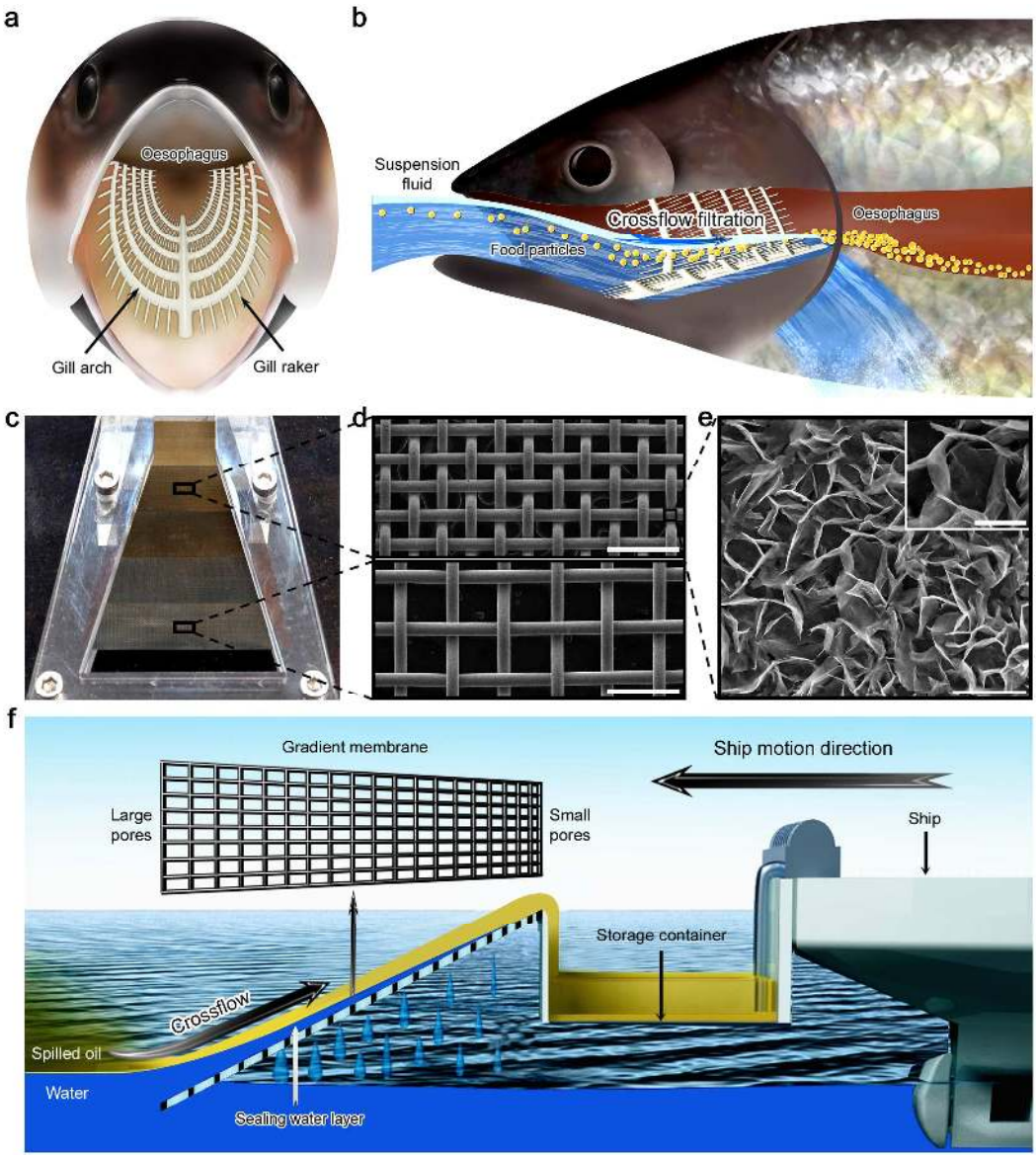

Figure 1. Crossflow filtration in fish gills and bioinspired crossflow collection of spilled oil. (a) Gradient gill structure in suspension-feeding fishes. (b) Illustration of crossflow filtration in fish gills, showing that the suspension fluid flows parallel to the gill surface with water gradually permeating through the spaces and food particles concentrated and transported to the oesophagus. (c) Gradient membrane that consists of five meshes arranged in descending order of pore size from the bottom to the top (150, 120, 90, 60 and 30 μm). **(**d) Large (bottom) and small pore (top) regions of the gradient membrane. Scale bars, 300 μm. (e) Ultrathin Co_3O_4 nanosheets coated on the wire surface, which form numerous enclosed cells (inset). Scale bars, 2 μm and 1 μm (inset). (f) Illustration of bioinspired crossflow collection of spilled oil. As the oil/water flows parallel to the gradient membrane surface (note large pores at the bottom and small pores at the top), water gradually passes through the pores, while oil is transported and finally collected for storage. In crossflow collection, a water layer seals the membrane surface, which plays a vital role in repelling the oil and protecting the membrane.

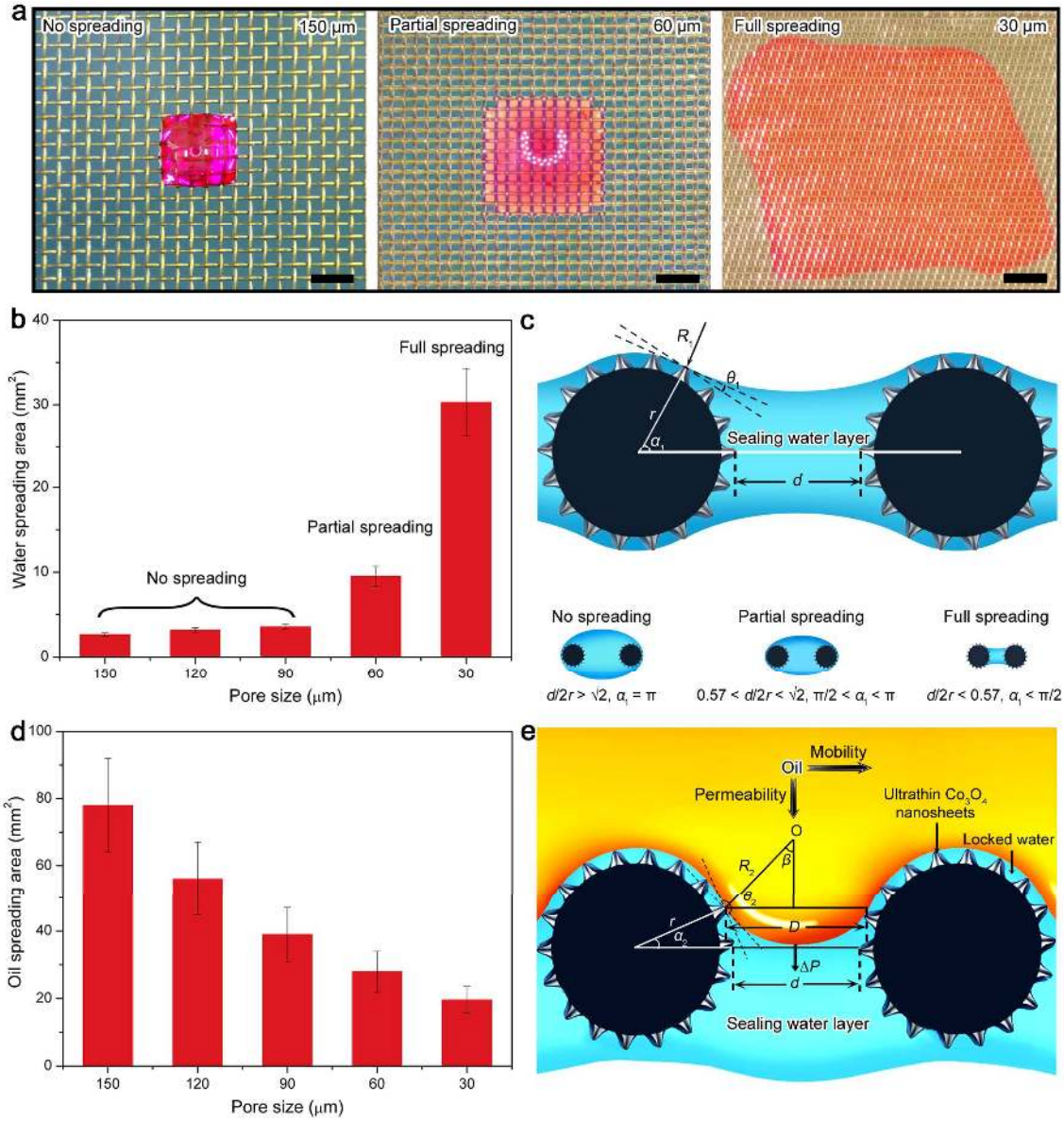

Figure 2. Formation and oil-repellency of the water-sealed membranes with different pore sizes at the extreme state. (a) Spreading behavior of a water droplet (1 μL, dyed with Rhodamine B) showing three different states—no spreading, partial spreading and full spreading. Scale bars, 0.5 mm. (b) Water spreading area as a function of pore size. (c) Schematic illustration showing the formation of the sealing water layer on two parallel wires. The final spreading state depends only on the value of $d/2r$. (d) Oil (anti-wear hydraulic fluid, 5 μL) spreading area on water-sealed membranes as a function of pore size. (e) Schematic illustration explaining the oil-repellency (P) of the water layer by the Laplace equation: $P = \Delta P = 4\gamma_{L_1L_2}\sin(\theta_2 - \pi/2 - \alpha_2)/[2r(1-\cos\alpha_2) + d]$.

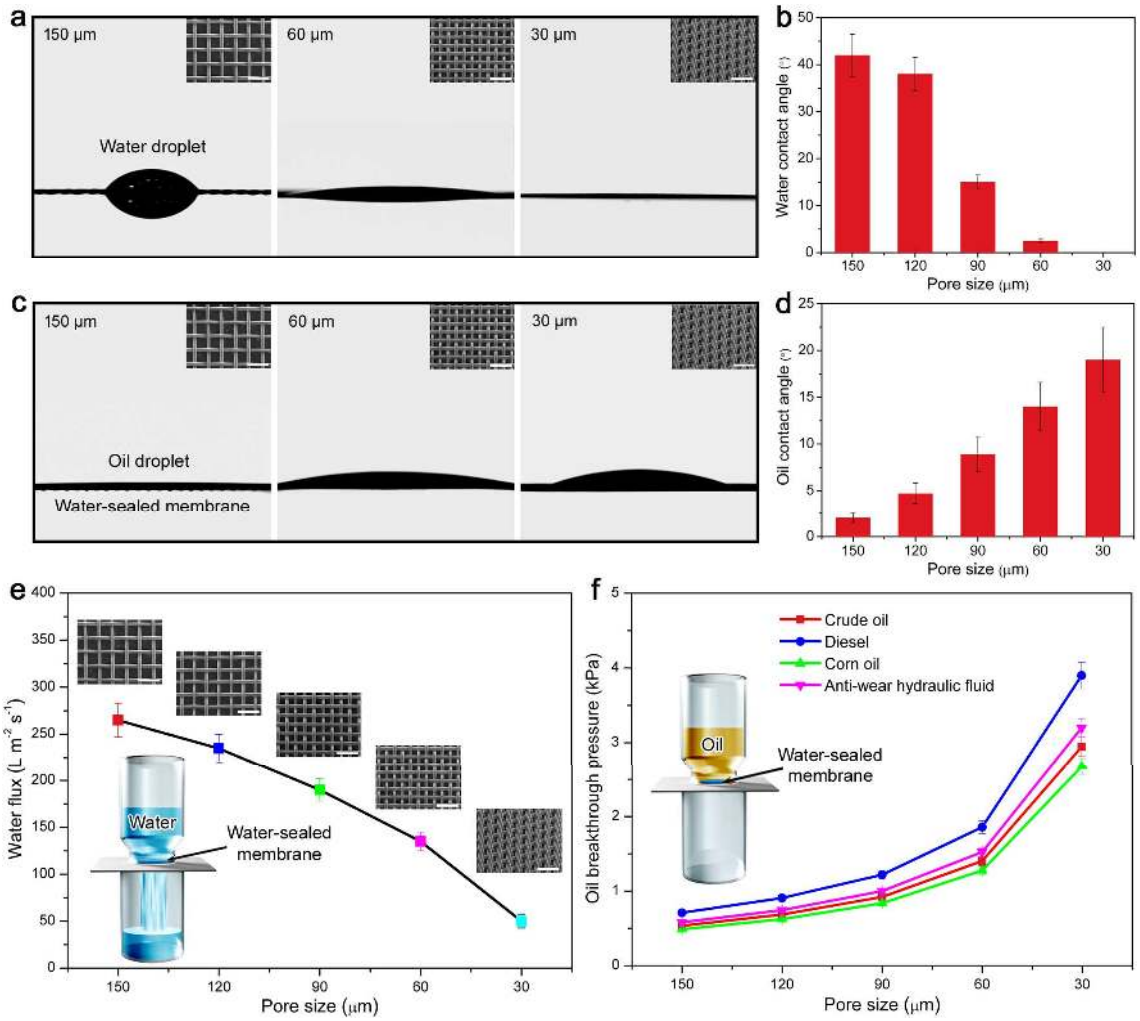

Figure 3. Wetting and permeating behaviors of water and oil on horizontally-placed membranes. (a) Wetting behavior of a water droplet (3 μL) on membranes with different pore sizes (with insets displaying their corresponding SEM images, scale bars: 300 μm). (b) Water contact angles. (c) Wetting behavior of an oil droplet (anti-wear hydraulic fluid, 5 μL) on water-sealed membranes. (d) Oil contact angles. (e) Water flux as a function of pore size (water pressure, 0.15 kPa). (f) Oil breakthrough pressure as a function of pore size.

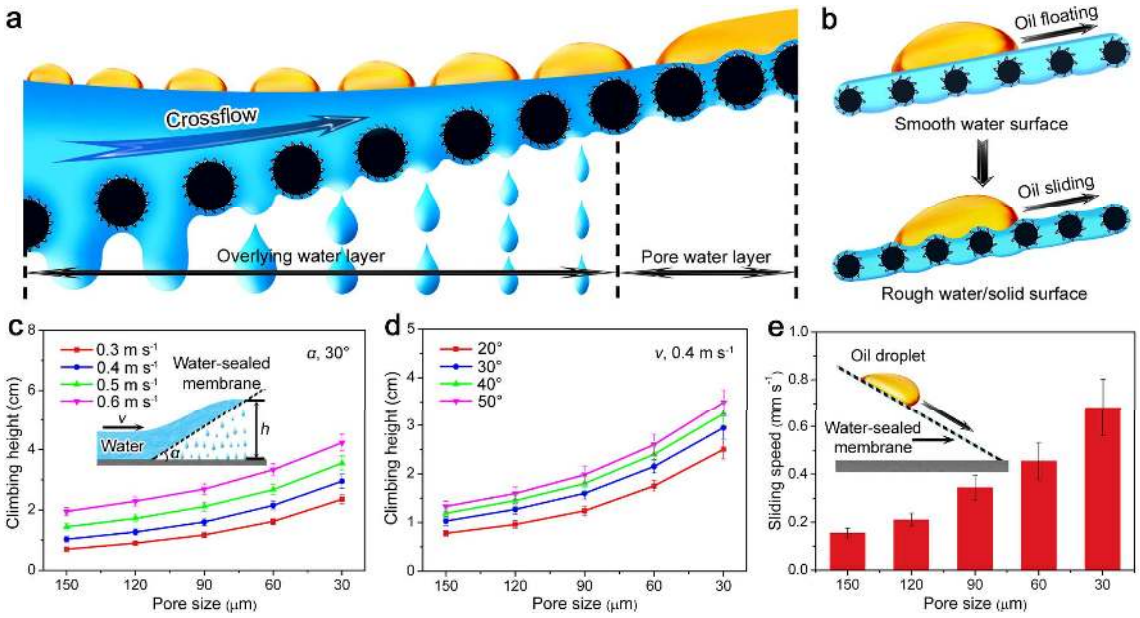

Figure 4. Mobility of water and oil on tilted membranes in crossflow collection. (a) Schematic illustration showing the evolution of the sealing water layer from overlying on the surface to being trapped in the pores. (b) The oil mobility exhibits two stages: 'oil floating' on a smooth water surface (top), and 'oil sliding' on a rough water/solid surface (bottom). (c) Climbing height of a water current (0.5 cm in thickness) as a function of pore size and current speed (membrane tilt, 30°). (d) Water climbing height as a function of pore size and membrane tilt (current speed, 0.4 m s^{-1}). (e) Sliding speed of an oil droplet (anti-wear hydraulic fluid, 20 μL) on water-sealed membranes (membrane tilt, 30°).

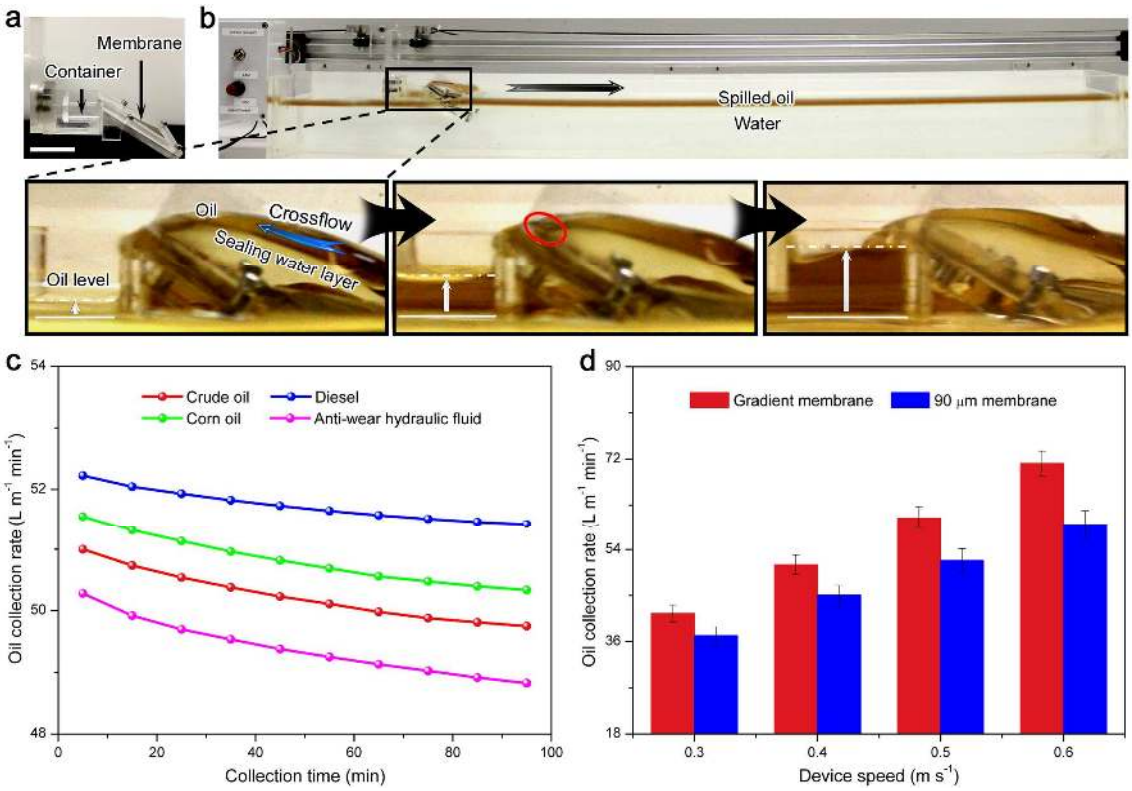

Figure 5. Laboratory demonstration of the crossflow spilled oil collection. (a) Optical image of a laboratory-scale demonstration device that consists of a gradient membrane and an oil container. Scale bar, 3 cm. (b) Dynamic process of the crossflow spilled oil collection (taking crude oil as an example). The enlarged images at the bottom clearly display the water layer (with the red ellipse marking the oil/water/solid region), the climbing oil and the collected oil. (c) Collection efficiency and stability for different types of oil (device speed, 0.4 m s^{-1}). (d) Comparison in terms of collection efficiency (crude oil) between the gradient membrane (average pore size, 90 μm) and a single-pore-size membrane (90 μm) at different device speeds.

ASSOCIATED CONTENT

Supporting Information

The Supporting Information is available free of charge on the ACS Publications website at DOI:

Additional results

AUTHOR INFORMATION

Corresponding Author

*E-mail: tiandl@buaa.edu.cn.

*E-mail: ziqi.sun@qut.edu.au.

ORCID

Notes

The authors declare no competing financial interest.

ACKNOWLEDGMENTS

The authors are grateful for financial support from the Australian Research Council (ARC) Discovery Project (DP160102627), the ARC for a Discovery Early Career Researcher Award grant (DE150100280), the UOW-BUAA Joint Research Centre, the Chinese National Natural Science Foundation (21671012, 21373001, 21601013), Beijing Natural Science Foundation (2172033), the 973 Program (2013CB933004), the China Scholarship Council (201306025005), the Fundamental Research Funds for the Central Universities (YWF-16-HHXY-001, YWF-15-HHXY-012, FRF-BR-15-023A), an Australian Postgraduate Award, and an International Postgraduate Research Scholarship.

REFERENCES

1. Yin, F.; Hayworth, J. S.; Clement, T. P. A Tale of Two Recent Spills—Comparison of 2014 Galveston Bay and 2010 Deepwater Horizon Oil Spill Residues. *PLOS ONE* **2015**, *10*, 1-17.
2. Camilli, R.; Reddy, C. M.; Yoerger, D. R.; Mooy, B. A. S. V.; Jakuba, M. V.; Kinsey, J. C.; McIntyre, C. P.; Sylva S. P.; Maloney, J. V. Tracking Hydrocarbon Plume Transport and Biodegradation at Deepwater Horizon. *Science* **2010**, *330*, 201-204.
3. Peterson, C. H.; Rice, S. D.; Short, J. W.; Eslter, D.; Bodkin, J. L.; Ballachey B. E.; Irons, D. B. Long-Term Ecosystem Response to the Exxon Valdez Oil Spill. *Science* **2003**, *302*, 2082-2086.
4. Crone, T. J.; Tolstoy, M. Magnitude of the 2010 Gulf of Mexico Oil Leak. *Science* **2010**, *330*, 634.
5. Nordvik, A. B.; Simmons, J. L.; Bitting, K. R.; Lewis, A.; Stromkristiansen, T. Oil and Water Separation in Marine Oil Spill Clean-up Operations. *Spill Sci. Technol. Bull.* **1996**, *3*, 107-122.
6. Choi, H.-M.; Cloud, R. M. Natural Sorbents in Oil Spill Cleanup. *Environ. Sci. Technol.* **1992**, *26*, 772-776.
7. Mullin, J. V.; Champ, M. A. Introduction/Overview to *In Situ* Burning of Oil Spills. *Spill Sci. Technol. Bull.* **2003**, *8*, 323-330.
8. Nyankson, E.; DeCuir, M. J.; Gupta, R. B. Soybean Lecithin as a Dispersant for Crude Oil Spills. *ACS Sustainable Chem. Eng.* **2015**, *3*, 920-931.
9. Ron, E. Z.; Rosenberg, E. Enhanced Bioremediation of Oil Spills in the Sea. *Curr. Opin. Biotechnol.* **2014**, *27*, 191-194.

10. Whitfield, J. How to Clean a Beach. *Nature* **2003**, *422*, 464-466.
11. Stout, S. A.; Payne, J. R. Chemical Composition of Floating and Sunken *In-Situ* Burn Residues from the Deepwater Horizon Oil Spill. *Mar. Pollut. Bull.* **2016**, *108*, 186-202.
12. Liu, T; Kim, C.-J. Turning a Surface Superrepellent Even to Completely Wetting Liquids. *Science* **2016**, *346*, 1096-1100.
13. Li, J.; Qin, Q. H.; Shah, A.; Ras, R. H. A.; Tian, X.; Jokinen, V. Oil Droplet Self-Transportation on Oleophobic Surfaces. *Sci. Adv.* **2016**, *2*, e1600148.
14. Golovin, K.; Kobaku, S. P. R.; Lee, D. H.; DiLoreto, E. T.; Mabry, J. M.; Tuteja, A. Designing Durable Icephobic Surfaces. *Sci. Adv.* **2016**, *2*, e1501496.
15. Tsujii, K.; Yamamoto, T.; Onda, T.; Shibuichi, S. Super Oil-Repellent Surfaces. *Angew. Chem. Int. Ed. Engl.* **1997**, *36*, 1011-1012.
16. Xue, Z.; Cao, Y.; Liu, N.; Feng, L.; Lei, J. Special Wettable Materials for Oil/Water Separation. *J. Mater. Chem. A* **2014**, *2*, 2445-2460.
17. Tuteja, A.; Choi, W.; Ma, M.; Mabry, J. M.; Mazzella, S. A.; Rutledge, G. C.; Mckinley, G. H.; Cohen, R. E. Designing Superoleophobic Surfacees. *Science* **2007**, *318*, 1618-1622.
18. Lu, Y.; Sathasivam, S.; Song, J.; Crick, C. R.; Carmalt, C. J.; Parkin, I. P. Robust Self-Cleaning Surfaces That Function When Exposed to Either Air or Oil. *Science* **2015**, *347*, 1132-1135.
19. Chen, K.; Zhou, S.; Wu, L. Self-Healing Underwater Superoleophobic and Antibiofouling Coatings Based on the Assembly of Hierarchical Microgel Spheres. *ACS Nano* **2016**, *10*, 1386-1394.

20. Yuan, J.; Liu, X.; Akbulut, O.; Hu, J.; Suib, S. L.; Kong, J.; Stellacci, F. Superwetting Nanowires Membranes for Selective Absorption. *Nat. Nanotech.* **2008**, *3*, 332-336.

21. Lei, W.; Portehault, D.; Liu, D.; Qin, S.; Chen, Y. Porous Boron Nitride Nanosheets for Effective Water Cleaning. *Nat. Commun.* **2013**, *4*, 1777.

22. Jayaramulu, K.; Datta, K. K. R.; Rosler, C.; Petr, M.; Otyepka, M.; Zboril, R.; Fischer, R. A. Biomimetic Superhydrophobic/Superoleophilic Highly Fluorinated Graphene Oxide and ZIF-8 Composites for Oil-Water Separation. *Angew. Chem. Int. Ed.* **2016**, *55*, 1178-1182.

23. Chen, N.; Pan, Q. Versatile Fabrication of Ultralight Magnetic Foams and Application for Oil-Water Separation. *ACS Nano* **2013**, *7*, 6875-6883.

24. Feng, L.; Zhang, Z.; Mai, Z.; Ma, Y.; Liu, B.; Jiang, L.; Zhu, D. A Super-Hydrophobic and Super-Oleophilic Coating Mesh Film for the Separation of Oil and Water. *Angew. Chem. Int. Ed.* **2004**, *43*, 2012-2014.

25. Chu, Z.; Feng, Y.; Seeger, S. Oil/Water Separation with Selective Superantiwetting/Superwetting Surface Materials. *Angew. Chem. Int. Ed.* **2015**, *54*, 2328-2338.

26. Zhang, W.; Liu, N.; Cao, Y.; Chen, Y.; Xu, L.; Lin, X.; Feng, L. A Solvothermal Route Decorated on Different Substrates: Controllable Separation of an Oil/Water Mixture to a Stabilized Nanoscale Emulsion. *Adv. Mater.* **2015**, *27*, 7349-7355.

27. Gao, C.; Sun, Z.; Li, K.; Chen, Y.; Cao, Y.; Zhang, S.; Feng, L. Intergrated Oil Separation and Water Purification by a Double-Layer TiO_2-Based Mesh. *Energy Environ. Sci.* **2013**, *6*, 1147-1151.

28. He, K.; Duan, H.; Chen, G. Y.; Liu, X.; Yang, W.; Wang, D. Cleaning of Oil Fouling with Water Enabled by Zwitterionic Polyelectrolyte Coatings: Overcoming the Imperative Challenge of Oil-Water Separation Membranes. *ACS Nano* **2015**, *9*, 9188-9198.

29. Kwon, G.; Kota, A. K.; Li, Y.; Sohani, A.; Mabry, J. M.; Tuteja, A. On-Demand Separation of Oil-Water Mixture. *Adv. Mater.* **2012**, *24*, 3666-3671.

30. Ju, G.; Cheng, M.; Shi, F. A pH-Responsive Smart Surface for the Continuous Separation of Oil/Water/Oil Ternary Mixtures. *NPG Asia Mater.* **2014**, *6*, e111.

31. Xue, Z.; Wang, S.; Lin, L.; Liu, M.; Feng, L.; Jiang, L. A Novel Superhydrophilic and Underwater Superoleophobic Hydrogel-Coated Mesh for Oil/Water Separation. *Adv. Mater.* **2011**, *23*, 4270-4273.

32. Zhang, F.; Zhang, W. B.; Shi, Z.; Wang, D.; Jin, J.; Jiang, L. Nanowire-Haired Inorganic Membranes with Superhydrophilicity and Underwater Ultralow Adhesive Superoleophobicity for High-Efficiency Oil/Water Separation. *Adv. Mater.* **2013**, *25*, 4192-4198.

33. Kota, A. K.; Kwon, G.; Choi, W.; Mabry, J. M.; Tuteja, A. Hygro-Responsive Membranes for Effective Oil-Water Separation. *Nat. Commun.* **2012**, *3*, 1025.

34. Field, R. W. Surface Science: Separation by Reconfiguration. *Nature* **2012**, *489*, 41-42.

35. Wen, Q.; Di, J.; Jiang, L.; Yu, J.; Xu, R. Zeolite-Coated Mesh Film for Efficient Oil-Water Separation. *Chem. Sci.* **2013**, *4*, 591-595.

36. Du, R.; Gao, X.; Feng, Q.; Zhao, Q.; Li, P.; Deng, S.; Shi, L.; Zhang, J. Microscopic Dimensions Engineering: Stepwise Manipulation of the Surface Wettability on 3D Substrates for Oil/Water Separation. *Adv. Mater.* **2016**, *28*, 936-942.

37. Gao, S.; Sun, J.; Liu, P.; Zhang, F.; Zhang, W.; Yuan, S.; Li, J.; Jin, J. A Robust Polyionized Hydrogel with an Unprecedented Underwater Anti-Crude-Oil-Adhesion Property. *Adv. Mater.* **2016**, *28*, 5307-5314.

38. Brainerd, E. L. Caught in the Crossflow. *Nature* **2001**, *412*, 387-388.

39. Hoogenboezem, W.; Lammens, E. H. R. R.; MacGillavry, P. J.; Sibbing, F. A. Prey Retention and Sieve Adjustment in Filter-Feeding Bream (Abramis Brama) (Cyprinidae). *Can. J. Fish. Aquat. Sci.* **1993**, *50*, 465-471.

40. Belfort, G.; Davis, R. H.; Zydney, A. L. The Behavior of Suspensions and Macromolecular Solutions in Crossflow Microfiltration. *J. Membr. Sci.* **1994**, *96*, 1-58.

41. Sanderson, S. L.; Cheer, A. Y.; Goodrich, J. S.; Graziano, J. D.; Callan, W. T. Crossflow Filtration in Suspension-Feeding Fishes. *Nature* **2001**, *412*, 439-441.

42. Leong, S. C.; Chen, X. B.; Lee, H. P.; Wang, D. Y. A Review of the Implications of Computational Fluid Dynamic Studies on Nasal Airflow and Physiology. *Rhinology* **2010**, *48*, 139-145.

43. Leordean, C.; Campean, V.; Astilean, S. Surface-Enhanced Raman Scatterin (SERS) Analysis of Urea Trace in Urine, Fingerprint, and Tear Samples. *Spectrosc. Lett.* **2012**, *45*, 550-555.

44. Yildiz, E. Phosphate Removal from Water by Fly Ash Using Crossflow Microfiltration. *Sep. Purif. Technol.* **2004**, *35*, 241-252.

45. Yuan, Y.; Kilduff, J. E. Effect of Colloids on Salt Transport in Crossflow Nanofiltration. *J. Membr. Sci.* **2010**, *346*, 240-249.

46. Ji, H. M.; Samper, V.; Chen, Y.; Heng, C. K.; Lim, T. M.; Yobas, L. Silicon-Based Microfilters for Whole Blood Cell Separation. *Biomed Microdev.* **2008**, *10*, 251-257.

47. Moslehyani, A.; Mobaraki, M.; Ismail, A. F.; Matsuura, T.; Hashemifard, S. A.; Othman, M. H. D.; Mayahi, A.; DashtArzhandi, M. R.; Soheimoghaddam, M.; Shamsaei, E. *React. Funct. Polym.* **2015**, *95*, 80-87.

48. Sun, Z.; Liao, T.; Dou, Y.; Hwang, S. M.; Park, M.-S.; Jiang, L.; Kim, J. H.; Dou, S. X. Generalized Self-Assembly of Scalable Two-Dimensional Transition Metal Oxide Nanosheets. *Nat. Commun.* **2014**, *5*, 3813.

49. Princen, H. M. Capillary Phenomena in Assemblies of Parallel Cylinders □. Liquid Columns Between Horizontal Parallel Cylinders. *J. Colloid Interface Sci.* **1970**, *34*, 171-184.

50. Duprat, C.; Protiere, S.; Beebe, A. Y.; Stone, H. A. Wetting of Flexible Fibre Arrays. *Nature* **2012**, *482*, 510-513.

51. Lafuma, A.; Quere, D. Superhydrophobic States. *Nat. Mater.* **2003**, *2*, 457-460.

52. Hou, X.; Hu, Y.; Grinthal, A.; Khan, M.; Aizenberg, J. Liquid-Based Gating Mechanism with Tunable Multiphase Selectivity and Antifouling Behaviour. *Nature* **2015**, *519*, 70-73.

53. Nosonovsky, M. Slippery When Wetted. *Nature* **2011**, *477*, 412-413.

54. Wong, T.-S.; Kang, S. H.; Tang, S. K. Y.; Smythe, E. J.; Hatton, B. D.; Grinthal, A.; Aizenberg, J. Bioinspired Self-Repairing Slippery Surfaces with Pressure-Stable Omniphobicity. *Nature* **2011**, *477*, 443-447.

55. Yao, X.; Hu, Y.; Grinthal, A.; Wong, T.-S.; Mahadevan, L.; Aizenbergy, J. Adaptive Fluid-Infused Porous Films with Tunable Transparency and Wettability. *Nat. Mater.* **2013**, *12*, 529-534.

GRAPHICAL TABLE OF CONTENTS

Inspired by the crossflow filtration behavior of fish gill, we propose a novel crossflow approach via a hydrophilic, titled gradient membrane for the collection of spilled oil. Owing to a water layer that seals the membrane pores, this bioinspired crossflow approach enables highly efficient and continuous spilled oil collection, which is very promising for the cleanup of large-scale oil spills.